A creep rupture model accounting for cavitation at sliding grain boundaries

Giessen, Erik van der; Tvergaard, Viggo

Published in:
International Journal of Fracture

DOI:
10.1007/BF00036629

International Journal of Fracture **48**: 153–178, 1991.

A creep rupture model accounting for cavitation at sliding grain boundaries

ERIK van der GIESSEN[1] and VIGGO TVERGAARD
Department of Solid Mechanics, The Technical University of Denmark, Lyngby, Denmark;
[1]*present address: Department of Mechanical Engineering, Delft University of Technology, Delft, The Netherlands*

Received 31 July 1989; accepted in revised form 27 March 1990

Abstract. An axisymmetric cell model analysis is used to study creep failure by grain boundary cavitation at facets normal to the maximum principal tensile stress, taking into account the influence of cavitation and sliding at adjacent inclined grain boundaries. It is found that the interaction between the failure processes on these two types of adjacent facets reduces the failure time significantly when cavitation is creep constrained. In all cases the time to cavity coalescence on transverse facets appears to be a useful lower bound measure of the material life-time. Sliding at the boundaries of the central grain of the cell model is accurately represented; but in some computations a stress enhancement factor is used to incorporate also the effect of sliding between surrounding grains. The influence of grain boundary viscosity is included in the model and it is found that even in the absence of sliding, cavitation on inclined boundaries may significantly reduce the failure time.

1. Introduction

In polycrystalline metals undergoing creep at high temperatures, failure occurs mainly by the nucleation and growth of microscopic cavities on the grain boundaries. Experiments show that cavitation occurs most rapidly on grain boundary facets normal to the maximum principal tensile stress direction, so that cavity coalescence leads to micro-cracks at these facets (Hull and Rimmer [1], Cocks and Ashby [2], Argon [3]). The final intergranular creep fracture occurs as these micro-cracks link up.

Much work has been devoted to studying cavity growth on facets normal to the maximum principal stress. Growth by grain boundary diffusion alone is part of the rigid grains model [1], and the combined effect of diffusion and dislocation creep of the surrounding material has been incorporated in detailed numerical studies of the growth of a single cavity (Needleman and Rice [4], Sham and Needleman [5]). Diffusive cavity growth on a few facets needs to be accommodated by creep deformation of the surrounding material, which may give a constraint on the growth rate [6]. Such creep constrained cavitation has been analysed by Rice [7], using a penny-shaped crack model of a cavitating grain boundary facet in a creeping solid, and subsequently this model has been extended to include other mechanisms [8, 9]. A number of approaches to creep cavitation have been discussed by Cocks and Leckie [10] and Riedel [11].

The time required for the formation of an open micro-crack by cavity coalescence on an average cavitating facet has been used in many investigations as a measure of the creep life-time; but this estimate neglects the last part of the life-time, during which the micro-cracks link up. For creep constrained conditions Riedel [12] has questioned the relevance of the time to coalescence as a measure of the life-time, because in these circumstances the

stress state near the cavitating facet is identical to that near an open micro-crack. Since the stress state is essentially unaffected by the onset of coalescence in the course of the process, the speed of linking up processes will also be essentially unaffected, and therefore Riedel expects that the time to coalescence has no particular significance for the life-time. However, Riedel [12] does find that experimental rupture data correlate rather well with predictions based on creep constrained cavitation models.

The most likely mechanisms for linking up of micro-cracks during the creep rupture process are grain boundary sliding or cavitation on intermediate grain boundary facets which are significantly inclined to the direction of maximum principal stress. The effect of free grain boundary sliding on creep rupture processes has been investigated by Anderson and Rice [13] and Tvergaard [9, 14, 15]. A preliminary study of the additional effect of cavitation on the sliding grain boundaries has been carried out by Van der Giessen and Tvergaard [16].

In the present paper the combined influence of cavitation and grain boundary sliding is studied on the basis of numerical solutions for an axisymmetric model problem. Sliding is modelled by a linear viscous relationship [17], so that the results for free sliding obtained in [16] correspond to the limit of zero boundary viscosity, while essentially no sliding results from taking a relatively high boundary viscosity. The rate of grain boundary diffusion is varied so that the results include the range of creep constrained cavitation as well as unconstrained cavitation. Furthermore, the effects of different stress states and of sliding enhanced creep are considered.

2. Problem formulation

The ultimate goal in a study of creep failure mechanisms is the determination of the actual life-time. Therefore, having studied cavitation and micro-crack formation at the grain boundary facets most critically oriented in the material, a natural next step is to consider failure mechanisms on the adjacent grain boundary facets in order to attempt a description of the final part of the life-time. The model problem to be analysed here extends the description of failure to the neighbouring facets; but the full fracture process is still not described.

Another motivation for the present model study is to investigate the relevance of the creep constrained cavitation model to the rupture life-time, as discussed by Riedel [12]. It will be seen that the time to coalescence during creep constrained cavitation is reduced by the early activation of linking up processes on adjacent facets; but this time does provide a relevant lower bound to the rupture time.

The axisymmetric model problem to be analysed here (Fig. 1) is an extension of the model used by Tvergaard [9] to study the effect of free grain boundary sliding on the rate of cavity growth. Cavitation on the freely sliding grain boundaries was included in the model by Van der Giessen and Tvergaard [16], and the present paper gives a further extension to consider the effects of non-zero grain boundary viscosity and of sliding enhanced creep in part of the model volume for reasons to be discussed later.

In the axisymmetric model problem the region ABCD analysed has an initial radius A_0 and initial height B_0, as shown in Fig. 1a, and the maximum principal tensile stress is taken to be in the axial direction (the x^1-direction). The main cavitating grain boundary facet AP

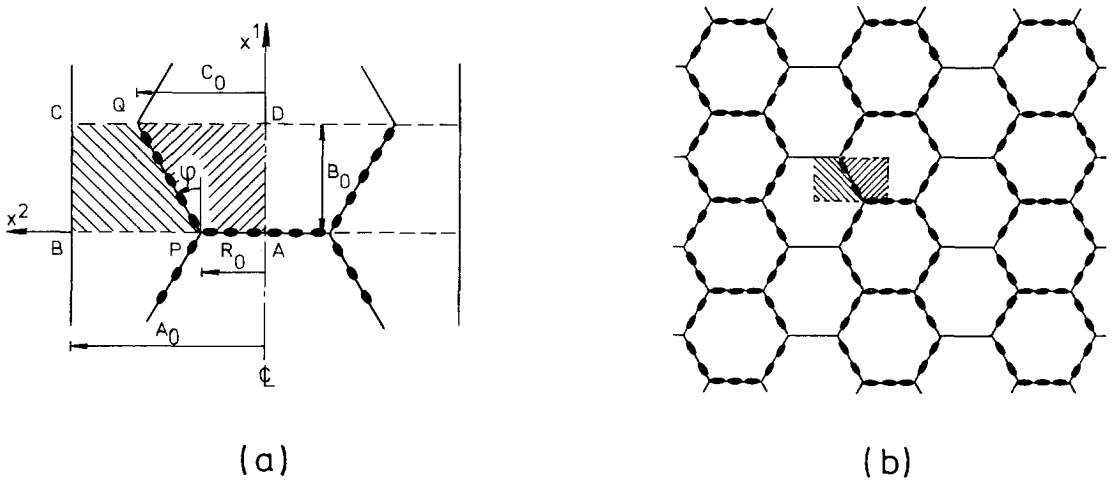

Fig. 1. (a) Axisymmetric model problem used to study the effect of cavitation and sliding at inclined grain boundaries; only the hatched region is analysed. (b) The type of periodic array of cavitated grain boundary facets modelled.

with initial radius R_0 is normal to the maximum principal tensile stress, and cavitation is also considered on the adjacent inclined grain boundaries PQ, where sliding takes place. Half of the central grain in the model is represented by a truncated cone APQD, while the external ring of material PBCQ represents part of a number of grains surrounding the central grain of the model.

As has been discussed by Tvergaard [9] the axisymmetric model problem represents a periodic array of grains, in which not all grain boundary facets normal to the maximum principal tensile stress are cavitated (see Fig. 1b). Thus, in Fig. 1a, AP represents a cavitated facet, while CQ represents a ring of non-cavitated facets surrounding the central grain of the model. Also, among the different grain boundary facets inclined to the axial direction, only those adjacent to a central facet such as AP are taken to be cavitated in the present model.

An alternative type of model has been suggested by Anderson and Rice [13], who analysed a case in which all facets normal to the maximum principal tensile stress are cavitated, while all other facets are subject to free sliding. Here, a full 3D-array of grains was represented by so-called Wigner–Seitz cells and an approximate solution was obtained by application of a stress-based variational principle. This fully cavitated state could represent a situation just before final failure, and in fact Anderson and Rice [13] do find much higher creep rates than those found by Tvergaard [9] for well separated cavitating facets.

Finite strains are accounted for in the analyses, using a convected coordinate formulation of the governing equations. The covariant components of the Lagrangian strain tensor are denoted by η_{ij}, with indices ranging from 1 to 3, and the contravariant components τ^{ij} of the Kirchhoff stress tensor on the current base vectors are defined in terms of the Cauchy stress tensor σ^{ij} by

$$\tau^{ij} = \sqrt{G/g}\,\sigma^{ij}. \tag{2.1}$$

Here, G and g are the determinants of the metric tensors G_{ij} and g_{ij} in the current configuration and in the reference configuration, respectively.

The material inside the grains is taken to deform by power-law creep in addition to elastic deformations. Thus, the creep part of the Lagrangian strain-rate is given by

$$\dot{\eta}_{ij}^{C} = \dot{\varepsilon}_e^{C} \frac{3}{2} \frac{s_{ij}}{\sigma_e}, \quad \dot{\varepsilon}_e^{C} = \dot{\varepsilon}_0 \left(\frac{\sigma_e}{\sigma_0} \right)^n, \tag{2.2}$$

where $\dot{\varepsilon}_0$ and σ_0 are reference strain-rate and stress quantities, and n is the creep exponent. The effective Mises stress $\sigma_e = \sqrt{3 s_{ij} s^{ij}/2}$ and the stress deviator $s^{ij} = \tau^{ij} - G^{ij}\tau_k^k/3$ are here specified directly in terms of the Kirchhoff stresses τ^{ij}, since the relative volume change $\sqrt{G/g} - 1$ is entirely due to elastic strains, which remain small.

The total strain-rate $\dot{\eta}_{ij}$ is taken to be the sum of the elastic part $\dot{\eta}_{ij}^{E}$ and the creep part $\dot{\eta}_{ij}^{C}$. Thus, with the elastic stress–strain relationship $\overset{\nabla}{\tau}{}^{ij} = R^{ijkl}\dot{\eta}_{kl}^{E}$, in terms of the Jaumann stress-rate $\overset{\nabla}{\tau}{}^{ij} = \dot{\tau}^{ij} + (G^{ik}\tau^{jl} + G^{jk}\tau^{il})\dot{\eta}_{kl}$, the constitutive relations for the elastic-creeping material can be written as

$$\overset{\nabla}{\tau}{}^{ij} = R^{ijkl}(\dot{\eta}_{kl} - \dot{\eta}_{kl}^{C}). \tag{2.3}$$

Grain boundaries can be modelled as thin layers, which slide in a Newtonian viscous way when a shear stress τ is applied in the plane of the boundary. Microscopic, atomistic aspects of such sliding have been treated by Ashby [17], who finds that the shear stress τ in the boundary is related to the relative sliding velocity $\dot{u}$ by an expression of the form

$$\tau = \eta_{\mathrm{B}} \frac{\dot{u}}{w}, \quad \eta_{\mathrm{B}} = \frac{kT}{8dD_{\mathrm{B}}}. \tag{2.4}$$

Here, the boundary viscosity η_{B} is defined for an idealized boundary of thickness w in terms of the boundary diffusion coefficient D_{B}, the atom size d, Boltzmann's constant k, and the absolute temperature T. Raj and Ashby [18] have analysed the influence of various irregularities in the grain boundary. For a periodic stepped boundary the viscosity (2.4b) is increased by a factor $(h/d)^2$, when h is the height of the steps, and a dispersion of particles or precipitates in the grain boundary raises the value of η_{B} in a similar manner [18, 19].

Plane strain model studies have been carried out by Crossman and Ashby [19] and Ghahremani [20] for polycrystalline aggregates with linearly viscous sliding at the grain boundaries and power law creep of the grains (see also discussion in [15]). These studies show that at high stresses sliding has a negligible influence on the overall creep rate, whereas at low stresses sliding is essentially free ($\tau = 0$), with higher overall creep strain-rates. Thus, during free sliding the macroscopic creep strain-rates can still be written as (2.2a), with the effective creep strain-rate (2.2b) replaced by a modified expression

$$\dot{\varepsilon}_e^{C} = \dot{\varepsilon}_0 \left(f^* \frac{\sigma_e}{\sigma_0} \right)^n, \tag{2.5}$$

where f^* is a stress enhancement factor ($f^* > 1$). Now, if free sliding takes place on the grain boundaries of a central grain, it seems plausible to assume that free sliding will occur also at the boundaries of all surrounding grains. This effect will be considered in an approximate way in some of the computations in the present paper by using the free

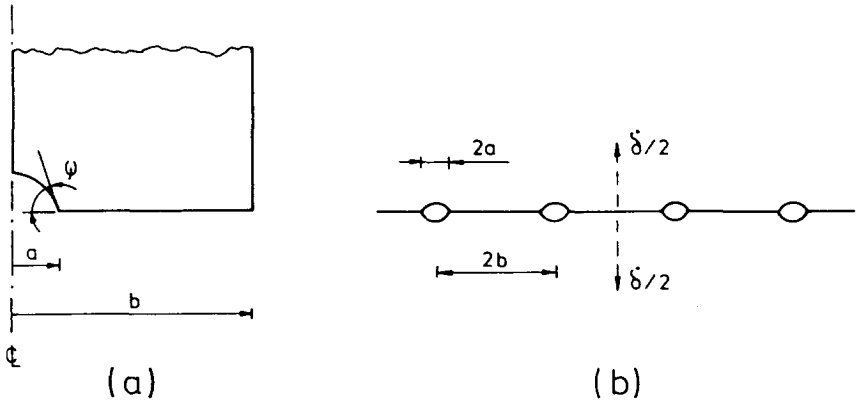

Fig. 2. (a) Geometry of a cavity in the spherical-caps shape; (b) Equally spaced cavities on a grain boundary.

sliding enhancement of creep described by (2.5) in the outer ring of material (PBCQ in Fig. 1a), which represents part of a number of grains surrounding the central grain of the model.

Grain boundary cavities tend to appear by continuous nucleation (Argon [3], Dyson [21]), so that the number of cavities is approximately proportional to the effective strain. Such continuous nucleation can be incorporated in the present model study (e.g. see [9]). However, for the illustration of other effects we here choose to focus on cases where the cavities are present from the beginning, thus representing cases where nucleation to a saturation level occurs at an early stage.

The grain boundary cavities grow by diffusion as well as by creep of the surrounding material. For a grain boundary facet normal to the maximum principal tensile stress, such as AP in Fig. 1a, approximate expressions for the rate of growth have been developed previously ([5], [8]). Thus, if the cavity radius is a, the average spacing is $2b$ and the cavities maintain the quasi-equilibrium spherical-caps shape (see Fig. 2), the volumetric growth rate $\dot{V}$ of a single cavity may be expressed as

$$\dot{V} = \dot{V}_1 + \dot{V}_2, \quad \text{for } \frac{a}{L} \leqslant 10, \quad f = \max\left\{\left(\frac{a}{b}\right)^2, \left(\frac{a}{a + 1.5L}\right)^2\right\}, \tag{2.6}$$

where

$$\dot{V}_1 = 4\pi\mathscr{D}\frac{\sigma_n - (1-f)\sigma_s}{\ln(1/f) - (3-f)(1-f)/2}, \tag{2.7}$$

$$\dot{V}_2 = \begin{cases} \pm 2\pi\dot{\varepsilon}_e^C a^3 h(\psi)\left[\alpha_n\left|\dfrac{\sigma_m}{\sigma_e}\right| + \beta_n\right]^n, & \text{for } \pm\dfrac{\sigma_m}{\sigma_e} > 1, \\ 2\pi\dot{\varepsilon}_e^C a^3 h(\psi)[\alpha_n + \beta_n]^n \dfrac{\sigma_m}{\sigma_e}, & \text{for } \left|\dfrac{\sigma_m}{\sigma_e}\right| \leqslant 1. \end{cases} \tag{2.8}$$

Here, $\mathscr{D} = D_B\delta_B\Omega/kT$ is the grain boundary diffusion parameter, with $D_B\delta_B$ denoting the boundary diffusivity and Ω the atomic volume. Furthermore, σ_n is the average stress normal

to the current orientation of the grain boundary in the vicinity of the void, and σ_m and σ_e are the average mean and effective stress, respectively. The constants are given by $\alpha_n = 3/2n$, $\beta_n = (n - 1)(n + 0.4319)/n^2$ and the cavity shape parameter h is defined by $h(\psi) = [(1 + \cos\psi)^{-1} - \frac{1}{2}\cos\psi]/\sin\psi$. The cavity tip angle ψ will be chosen as $\psi = 75°$ and the sintering stress σ_s in (2.7) will be neglected. The parameter

$$L = (\mathscr{D}\sigma_e/\dot{\varepsilon}_e^C)^{1/3} \tag{2.9}$$

in (2.6) serves as a stress and temperature dependent length scale as discussed by Needleman and Rice [4]. For $a/L < 0.1$ cavity growth is completely dominated by diffusion, whereas for higher values of a/L creep growth plays an increasing role. With $\dot{V}$ according to (2.6), the growth rate of the cavity radius is found as $\dot{a} = \dot{V}/(4\pi a^2 h(\psi))$.

Cavity growth on the inclined grain boundary PQ in Fig. 1a will be accompanied by a noticeable amount of sliding, unless the viscosity η_B in (2.4) is relatively large. Diffusional growth accompanied by grain boundary sliding may give rise to non-equilibrium void shapes showing inversion symmetry, as discussed by Argon and Chen [3, 22, 23], and may give an important contribution to accelerated cavity growth in the last stage of creep (see [23]). A first quantitative model of diffusive cavity growth on sliding grain boundaries was introduced recently by Chen [24]. This model has not yet reached a level of completeness that is sufficient for the present study, since the volumetric growth of cavities is unspecified and also the interaction with creep remains to be investigated. Therefore, we will assume here that cavity growth on the inclined grain boundary is such that it can be described approximately by the same growth relations (2.6–8) as for the quasi-equilibrium shape. According to [24] this is a reasonable approximation for relatively low sliding rates.

In the present analysis, we employ a continuous "smeared out" model of the cavitated grain boundary facets. Thus, a facet containing a discrete distribution of cavities is represented as a grain boundary layer to which a continuous distribution of the cavitation parameters a and b is attributed. Furthermore, the local thickness δ_c of this layer – or average separation between the two adjacent grains – is determined by the local values a and b according to $\delta_c = V/\pi b^2$. The growth rate of this thickness as specified by

$$\dot{\delta}_c = \frac{\dot{V}}{\pi b^2} - \frac{2V}{\pi b^2}\frac{\dot{b}}{b}, \tag{2.10}$$

is then determined by the volumetric growth rate of the cavities according to (2.6) and by the rate of change of the cavity spacing. Since, as discussed before, cavity nucleation is neglected here, the cavity spacing changes only due to straining of the material. The grain boundary area associated with each cavity is πb^2 (see Fig. 2a) and thus the number of cavities on a surface element $\mathrm{d}A$ of the grain boundary is $\mathrm{d}A/\pi b^2 = \text{const}$. It then follows by differentiation that the ratio $\dot{b}/b$ in (2.10) is given by

$$\frac{\dot{b}}{b} = \tfrac{1}{2}(\dot{\varepsilon}_2 + \dot{\varepsilon}_3), \tag{2.11}$$

where $\dot{\varepsilon}_2$ and $\dot{\varepsilon}_3$ are the local principal logarithmic strains at the grain boundary.

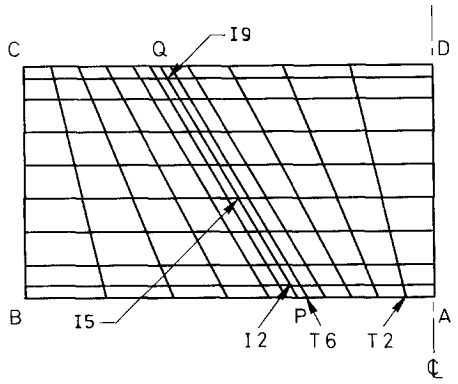

Fig. 3. Finite element mesh used in numerical analysis. Each quadrilateral is composed of four triangular subelements.

3. Method of analysis

The finite element model of the central grain APQD and the ring QPBC uses quadrilateral elements, each built up of four linear displacement triangular subelements arranged in a "crossed triangle" configuration. The mesh used in this study, depicted in Fig. 3, is composed of 6 × 9 quadrilateral elements in both the central grain and the surrounding ring.

The numerical solutions are obtained by a linear incremental method. At any discrete instant during the incremental analysis, rate equilibrium for each finite element is specified through the incremental form of the principle of virtual work:

$$\Delta t \int_V (\dot{\tau}^{ij}\delta\eta_{ij} + \tau^{ik}\dot{u}^j_{,k}\delta u_{j,i})\mathrm{d}V = \Delta t \int_S \dot{T}^i \delta u_i \,\mathrm{d}S - \left[\int_V \tau^{ij}\delta\eta_{ij}\mathrm{d}V - \int_S T^i \delta u_i \,\mathrm{d}S\right]. \quad (3.1)$$

Here, V and S are the volume and the surface, respectively, of the element in the reference configuration and Δt is the prescribed time increment. The bracketed terms in (3.1) vanish if the current state satisfies equilibrium. They are included in (3.1) as a correction to reduce drifting of the solution from the true equilibrium path due to the discrete time step.

In formulating the finite element equations, the stress rates $\dot{\tau}^{ij}$ in (3.1) are eliminated by means of the constitutive equations (2.3) for the creeping grains. As in earlier studies [8, 9, 14], a forward gradient method proposed by Pierce et al. [25] was used to increase the stable step size.

Special purpose finite elements are used to model the grain boundary layers along the inclined grain boundary PQ and the central facet AP. These so-called grain boundary elements are designed to allow for cavity growth and thickening of the grain boundary layer, as well as for viscous sliding of the adjacent grains relative to each other. At each step during the incremental procedure, the grain boundary layer is divided into elements as illustrated in Fig. 4. The strategy used is briefly discussed in Appendix A. Figure 4 shows a typical grain boundary element, which is defined as the segment $bc'cb'$ of the grain boundary layer between the two adjacent grain boundary nodes p and q. Introducing a local set of base vectors $\mathbf{e}_\alpha$ ($\alpha = 1, 2$), the rate of thickening of the grain boundary layer, $\dot{\delta}$, and the shearing

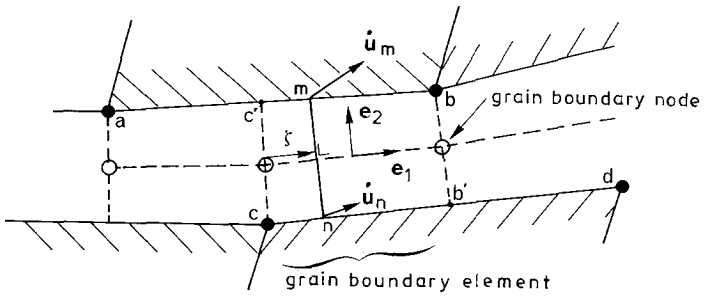

Fig. 4. Definition of grain boundary elements.

rate $\dot{\gamma}$ at a position within the grain boundary element specified by the local coordinate $\zeta \in [0, 1]$ are defined by

$$\dot{\delta} = (\dot{\mathbf{u}}_m - \dot{\mathbf{u}}_n) \cdot \mathbf{e}_2, \quad \dot{\gamma} = (\dot{\mathbf{u}}_m - \dot{\mathbf{u}}_n) \cdot \mathbf{e}_1, \tag{3.2}$$

where $\dot{\mathbf{u}}_m$ and $\dot{\mathbf{u}}_n$ are the velocity vectors at the associated points m and n on the edge of the adjacent quadrilaterals (see Fig. 4).

The normal stress σ_n and the shear stress τ at the grain boundary are in the finite element model determined by the constitutive behaviour of the grain boundary layer. The rate of thickening of the grain boundary layer due to cavity growth, $\dot{\delta}_c$, is specified by (2.10) and (2.6). However in the absence of cavitation the rate of thickening $\dot{\delta}$ should vanish, while at the same time sliding could still take place. As discussed in [14], it is convenient in a numerical analysis to treat this contact problem in an approximate way by introducing a fictitious layer of linear elastic springs normal to the grain boundary. Similarly we introduce a fictitious elastic spring layer against shearing, and describe grain boundary sliding by a visco-elastic relationship instead of by (2.4a). Thus, the constitution of each grain boundary element is specified in terms of the following rate equations:

$$\dot{\sigma}_n = k_n(\dot{\delta} - \dot{\delta}_c); \tag{3.3}$$

$$\dot{\tau} = k_s(\dot{\gamma} - \dot{\gamma}_v), \quad \dot{\gamma}_v = \frac{\tau}{\eta_B/w}, \tag{3.4}$$

with k_n and k_s the stiffnesses of the normal and shearing spring layers, respectively, and with $\dot{\delta}_c$ evaluated from (2.10). The deviations $\dot{\delta} - \dot{\delta}_c$ and $\dot{\gamma} - \dot{\gamma}_v$ introduced by these fictitious spring layers can be kept very small by using large values of k_n and k_s; here we used $k_n = k_s = 33.3E/A_0$ (E being Young's modulus of the grains).

The stresses σ_m and σ_e in the expression (2.8) for the volumetric cavity growth rate are calculated as averages of the values in the quadrilateral grain elements on either side of the grain boundary layer. The latter values are evaluated as averages over the four triangular subelements. For a given increment, the values of these stresses as well as the values of σ_n and τ to be used in (2.7) and (3.4), are calculated from the results of the previous increment. The rate $\dot{b}$ needed in (2.10) to evaluate $\dot{\delta}_c$ is at each increment calculated from (2.11) using the average velocity distribution on either side of the grain boundary layer in the previous increment.

The normal stress σ_n in the expression (2.7), needed to evaluate $\dot{\delta}_c$ according to (2.10), is obtained by simultaneous integration of the constitutive relationship (3.3). It was noted in earlier studies [8, 9] that small oscillations in σ_n tended to give rise to numerical instabilities which were remedied by a suitable amount of under-relaxation. Here, numerical stability has been improved by application of a forward gradient scheme in the integration of (3.3), just as in the integration of the constitutive equations for creep discussed before. The cavity growth contribution $\dot{\delta}_c$ to be used in (3.3) is expressed by a linear interpolation between the values at time t and $t + \Delta t$, respectively,

$$\dot{\delta}_c = (1 - \theta)\dot{\delta}_c^{(t)} + \theta\dot{\delta}_c^{(t+\Delta t)}; \quad \theta \in [0, 1], \tag{3.5}$$

where a Taylor series expansion is used to estimate $\dot{\delta}_c$ at $t + \Delta t$:

$$\dot{\delta}_c^{(t+\Delta t)} = \dot{\delta}_c^{(t)} + \frac{\partial \dot{\delta}_c}{\partial \sigma_n} \dot{\sigma}_n \Delta t. \tag{3.6}$$

Since the expression for $\dot{\delta}_c$ is very sensitive to variations of σ_n, the dependence on this parameter is included in the Taylor expansion (3.6), while the influence on σ_m etc. is neglected. Then the constitutive equations (3.3) (for time t) can be rewritten as

$$\dot{\sigma}_n = k_n^*(\dot{\delta} - \dot{\delta}_c); \tag{3.7}$$

with a modified time step dependent stiffness k_n^* given by

$$k_n^* = k_n \Big/ \left(1 + k_n \theta \frac{\partial \dot{\delta}_c}{\partial \sigma_n} \Delta t\right). \tag{3.8}$$

The computations here have been carried out with $\theta = 0.9$ which turned out to improve the numerical stability significantly (for $\theta = 0$, Eqns. (3.7–8) reduce to (3.3)).

A similar approach could easily be applied to the visco-elastic relation (3.4) for grain boundary sliding. However, in the calculations shown here, the time step remained sufficiently small to use the original formulation (3.4) without instability problems.

The finite element equations for the grain boundary elements are basically obtained again on the basis of an incremental virtual work condition similar to (3.1), but formulated with respect to the current configuration. However for these grain boundary elements we employ a geometrically linear formulation in which the convective contributions to the rate of internal virtual work are neglected. The results to be presented in Section 5 indicate that this is a reasonable approximation.

The boundary conditions used in the numerical model read

$$\left.\begin{aligned} \dot{u}^1 &= 0, \quad \dot{T}^2 = \dot{T}^3 = 0 && \text{along AB;} \\ \dot{u}^1 &= \dot{U}_{\mathrm{I}}, \quad \dot{T}^2 = \dot{T}^3 = 0 && \text{along CD;} \\ \dot{u}^2 &= \dot{U}_{\mathrm{II}}, \quad \dot{T}^1 = \dot{T}^3 = 0 && \text{along BC.} \end{aligned}\right\} \tag{3.9}$$

The boundary condition (3.9a) on AP refers to the midplane of the grain boundary layer (due to symmetry, only the top half of this layer needs to be analysed). The uniform displacements $\dot{U}_\mathrm{I}$ and $\dot{U}_\mathrm{II}$ in (3.9a–b) are determined so that the average true stresses σ_1 and σ_2 in the axial and radial directions,

$$\sigma_1 = \frac{2}{A^2}\int_0^{A_0} [T^1 x^2]_{x^1=B_0}\,\mathrm{d}x^2, \quad \sigma_2 = \frac{A_0}{AB}\int_0^{B_0} [T^2]_{x^2=A_0}\,\mathrm{d}x^1, \tag{3.10}$$

respectively, retain specified constant values. Here $A = A_0 + U_\mathrm{II}$ and $B = B_0 + U_\mathrm{I}$ are the current radius and height, respectively, of the region analysed. Macroscopic logarithmic strain-rates are defined by

$$\dot{E}_1 = \dot{U}_\mathrm{I}/B, \quad \dot{E}_2 = \dot{U}_\mathrm{II}/A. \tag{3.11}$$

Although a tensile stress state will be applied in the x^1-direction, $\sigma_1 > 0$, a compressive normal stress may occur in a region of the inclined boundary depending on the ratio σ_2/σ_1. In reality, cavities will not nucleate in this region. Since we assume cavities to be present from the beginning, they will close down in regions of compressive normal stress. For numerical convenience, cavities are considered to have closed completely when they have reached a minimum size which is taken here as the critical cavity size $a_c \simeq 2\gamma_s/\sigma_n \sin\psi$ for diffusive growth according to (2.7) [26], corresponding to a value of $\sigma_n = \sigma_1$ (γ_s is the surface free energy for the grain boundary).

As in previous studies [8, 9], coalescence of the cavities is taken to occur when the ratio a/b is close to unity. This is characteristic for cases where creep constrained cavity growth leads to very small normal stresses σ_n on cavitating grain boundary facets. In cases where σ_n is higher this will overestimate the time to cavity coalescence, since, as discussed by Cocks and Ashby [2], failure of the ligaments between cavities by ductile tearing or cleavage may occur at $a/b \simeq 0.5$.

4. A simplified model

In addition to the detailed finite element (FE) model discussed in the previous section, we will consider a much simplified model of the problem illustrated in Fig. 1. The purpose is to extract the main mechanisms of the problem to obtain a quick approximation of the full numerical results. The simple model may be considered an extension of the model discussed in [14] in a study of the influence of grain boundary sliding without cavitation.

The model analysed consists of two "elements" (2E), namely a central cylinder with initial radius $R_1 = (R_0 + C_0)/2$ and a ring with an inner radius R_1 and an outer radius A_0 in the initial state (see Fig. 5). In this so-called 2E model, all quantities are referred to the initial undeformed configuration so that nonlinear geometric effects are neglected. The modes of deformation are defined in terms of the prescribed displacement rates $\dot{u}^1 = \dot{U}_\mathrm{I}$ on CD and $\dot{u}^2 = \dot{U}_\mathrm{II}$ on BC [cf. (3.9)], uniform displacement-rates $\dot{u}_c^2$ and $\dot{u}_r^2$ along P′Q′ (see Fig. 5). at the outside of the cylinder and the inside of the ring, respectively, and the uniform axial displacement-rate $\dot{\delta}_t$ at the bottom AP′ of the cylinder due to cavity growth on the transverse

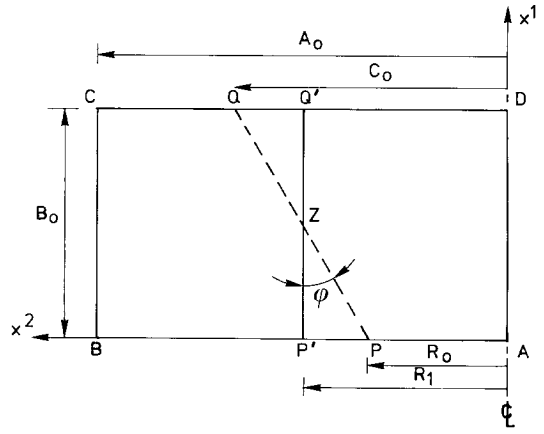

Fig. 5. Geometry of the simple 2E model: a central cylinder and a ring initially in contact at a radius R_1.

facet AP. The principal strain-rates $\dot{\varepsilon}_{\alpha c}$ and $\dot{\varepsilon}_{\alpha r}$ ($\alpha = 1, 2, 3$) in the cylinder and the ring, respectively, defined by

$$\dot{\varepsilon}_{1c} = \frac{\dot{U}_{\mathrm{I}} - \dot{\delta}_t}{B_0}, \quad \dot{\varepsilon}_{2c} = \dot{\varepsilon}_{3c} = \frac{\dot{u}_c^2}{R_1},$$

$$\dot{\varepsilon}_{1r} = \frac{\dot{U}_{\mathrm{I}}}{B_0}, \quad \dot{\varepsilon}_{2r} = \frac{\dot{U}_{\mathrm{II}} - \dot{u}_r^2}{A_0 - R_1}, \quad \dot{\varepsilon}_{3r} = \frac{\dot{U}_{\mathrm{II}} + \dot{u}_r^2}{A_0 + R_1}, \tag{4.1}$$

are assumed to represent averages of the actual strain-rates.

The thickness of the grain boundary layer along PQ as well as the relative sliding are assumed to vary linearly, such that they match the axial rate of displacement $\dot{\delta}_t$ at P. Thus, we introduce a rate of thickening $\dot{\delta}_i$ and a sliding rate $\dot{\gamma}$ in the 2E model as the corresponding values at the midpoint Z ($x^1 = B_0/2$, $x^2 = R_1$) of the inclined boundary:

$$\dot{\delta}_i = (\dot{u}_r^2 - \dot{u}_c^2)\cos\varphi + \tfrac{1}{2}\dot{\delta}_t \sin\varphi,$$

$$\dot{\gamma} = (\dot{u}_r^2 - \dot{u}_c^2)\sin\varphi - \tfrac{1}{2}\dot{\delta}_t \cos\varphi. \tag{4.2}$$

It follows immediately that in the absence of cavity growth on the inclined boundary, $\dot{\delta}_i = 0$, while sliding along PQ is completely prevented, $\dot{\gamma} = 0$, the 2E model requires $\dot{u}_c^2 = \dot{u}_r^2$ and $\dot{\delta}_t = 0$ so that cavity growth on the central facet cannot be represented in this case by the simple 2E model.

Dual to the strain-rates $\dot{\varepsilon}_{\alpha c}$ and $\dot{\varepsilon}_{\alpha r}$ defined in (4.1), stresses $\sigma_{\alpha c}$ and $\sigma_{\alpha r}$ are introduced which are taken as constants in the cylinder and the ring, respectively. The normal stress distributions on the transverse and inclined facets are represented by constant stresses σ_{nt} and σ_{ni}, respectively, and a constant shear stress τ is introduced as an approximation to the shear stress distribution on PQ. In Appendix B, the corresponding equilibrium equations are derived.

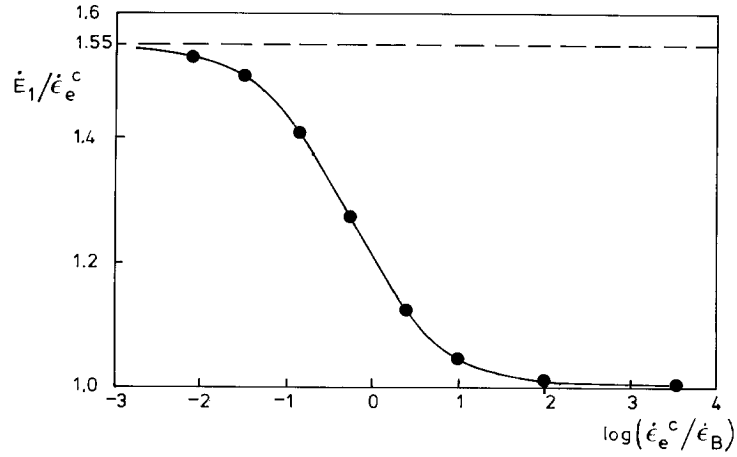

Fig. 6. Macroscopic logarithmic strain-rate vs the grain boundary viscosity at the inclined grain boundary.

The constitutive equations for the ring, in terms of $\sigma_{\alpha r}$ and $\dot{\varepsilon}_{\alpha r}$, and for the cylinder, in terms of $\sigma_{\alpha c}$ and $\dot{\varepsilon}_{\alpha c}$, can formally be derived from the general relationships (2.2) and (2.3). However, the stiffness of the system will be overestimated in the cases where there is sliding along the boundary PQ. As indicated by the analyses in [19] and [20], and found also in our FE computations, grain boundary sliding involves considerable stress redistributions inside the central grain and the surrounding ring which amplify the overall creep rate. In the case of free grain boundary sliding this gives rise to the factor f^* in (2.5). In the 2E model, the stress states in the cylinder and the ring are represented by uniform states, so that the above-mentioned local stress redistributions are not accounted for. Therefore, we explicitly incorporate the resulting enhanced creep rate by introducing an enhancement factor g_B such that the effective creep rate in either ring or cylinder is given by an expression

$$\dot{\varepsilon}_e^C = \dot{\varepsilon}_0 \left(g_B \frac{\sigma_e}{\sigma_0} \right)^n. \tag{4.3}$$

The value of g_B to be used for a given grain boundary viscosity can be calibrated with the results for the macroscopic strain-rates obtained from the FE analysis. A master curve to gauge the value of g_B for a given grain boundary viscosity will be presented in the next section (see Fig. 6). In analyses where also the effect of sliding enhanced creep in the ring PBCQ is considered, the value of g_B in the ring has to be replaced by $f^* g_B$ [cf. (2.5)].

The constitutive equations for both grain boundaries, in terms of σ_{nt} vs $\mathring{\delta}_n$, σ_{ni} vs $\mathring{\delta}_i$ and τ vs $\dot{\gamma}$, are taken according to (3.3) and (3.4). The mean and effective Mises stress σ_m and σ_e to be used in the evaluation of $\mathring{\delta}_c$ in (3.3) from (2.6–8) and (2.10) for the inclined boundary are taken as the average values over the cylinder and the ring. The Mises stress used for the transverse facet is taken equal to the Mises stress in the cylinder, but the mean stress inside the cylinder, $(\sigma_{1c} + 2\sigma_{2c})/3$, was found to underestimate the mean stress in the vicinity of the facet. A modified value $\sigma_m = (R_1/R_0)(\sigma_{1c} + 2\sigma_{2c})/3$ gave much better agreement with the FE results and was used instead.

Creep constrained cavity growth in this 2E model relies on a simple mechanism of redistribution of the macroscopic principal stress σ_1. First, the axial stress σ_1 is distributed

over the stresses σ_{1c} and σ_{1r} in the cylinder and the ring, respectively. The stress inside the central cylinder is distributed over the two grain boundary facet stresses σ_{nt}, σ_{ni} and τ. A constraint on cavity growth on the central facet in particular may arise as a result of the compatibility condition between the axial displacement of the top of the ring CQ′ and that of the cylinder Q′D, where both creep of the cylinder and cavity growth on AP contribute to the latter. This mechanism is reminiscent of Dyson's phenomenological one-dimensional two-bar model [27], but here axisymmetric stress states are considered and the interaction at inclined boundaries is taken into account.

In a macroscopically uniaxial stress state, the normal stress σ_{ni} on the inclined boundary is governed by contraction effects. It is expected then that $\sigma_{ni} < 0$ in situations where the creep constraint is active, since σ_{1c} will be considerably smaller than σ_{1r} and hence $\dot{\varepsilon}_{3r} < \dot{\varepsilon}_{3c}$. As a consequence, the simple model will not predict cavity growth on the inclined boundary when $\sigma_1 = 0$ (or, in fact, $\sigma_1 \leqslant 0$).

Though, as discussed above, the simple model cannot account for local stress redistributions inside the grains due to free sliding, it does predict the amplification of the normal stress σ_{nt} at the transverse facet AP due to the release of shear stresses on PQ. For a planar hexagonal array of grains, Rice [7] showed that this enhancement follows from mere equilibrium considerations and the results were used by Tvergaard [2] as a guide in presenting the constitutive theory account for free sliding based on an axisymmetric model. Here, σ_{nt} is not governed by equilibrium only, but has to be obtained by integration of the constitutive equations (3.3) during the incremental analysis.

In the following, results of this simple 2E model will be compared with results of the full numerical cell model analysis.

5. Results

As in [9, 16], the geometry of the model problem used for the results to be presented is taken to have $B_0/A_0 = 0.577$, $R_0/A_0 = 0.333$, $C_0/A_0 = 0.667$ and $\varphi = 30°$ (see Fig. 1b), so that a cross-section appears like that of a planar array of hexagonal grains. The material properties are specified by $n = 5$, Poisson's ratio $\nu = 0.3$ and surface free energy $\gamma_s/(EA_0) = 0.27 \times 10^{-7}$. The parameter $\dot{\varepsilon}_0/\sigma_0^n$ is used to set a time scale $t_R = \sigma_e/(E\dot{\varepsilon}_e^C)$ for a prescribed value $\sigma_e = |\sigma_1 - \sigma_2|$ of the macroscopic or average effective Mises stress and a corresponding value of $\dot{\varepsilon}_e^C$ according to (2.2b). The grain boundary viscosity is specified relative to the macroscopic creep rate in terms of the parameter $\dot{\varepsilon}_e^C/\dot{\varepsilon}_B$ where $\dot{\varepsilon}_B$ is defined by (cf. [20])

$$\dot{\varepsilon}_B = \dot{\varepsilon}_0 \Big/ \left(2\eta_B \frac{B_0}{w} \frac{\dot{\varepsilon}_0}{\sigma_0}\right)^{n/n-1}. \tag{5.1}$$

The free sliding limit is characterized by $\dot{\varepsilon}_e^C/\dot{\varepsilon}_B = 0$, while $\dot{\varepsilon}_e^C/\dot{\varepsilon}_B \to \infty$ in the limit of no sliding.

We begin by considering the effect of viscous grain boundary sliding on the macroscopic behaviour when cavitation is completely absent, since we will be needing some of the results in the subsequent analysis.

5.1. Viscous grain boundary sliding in absence of cavitation

The influence of viscous sliding along the inclined boundary is studied in terms of the macroscopic strain-rates $\dot{E}_1$ and $\dot{E}_2$. When there is no sliding along PQ, $\dot{\varepsilon}_B = 0$, the stress state within ABCD is uniform and the macroscopic strain-rate is equal to the effective creep strain-rate $\dot{\varepsilon}_e^C$ according to (2.2b) when elastic strains are neglected. Figure 6 shows the macroscopic strain-rate relative to this value $\dot{\varepsilon}_e^C$ as a function of the grain boundary viscosity specified in terms of $\dot{\varepsilon}_e^C/\dot{\varepsilon}_B$ [see (5.1)]. The curve has been obtained for a material subjected to uniaxial tension, $\sigma_2/\sigma_1 = 0$, but additional computations have indeed shown that the results are independent of σ_2/σ_1. The curve exhibits the typical S-shape [19, 20] where the influence of grain boundary sliding is negligible for $\dot{\varepsilon}_e^C/\dot{\varepsilon}_B > 10$ approximately and where sliding is virtually free for $\dot{\varepsilon}_e^C/\dot{\varepsilon}_B < 0.1$. For completely free sliding we find $\dot{E}_1/\dot{\varepsilon}_e^C = 1.55$, which corresponds to a value of the enhancement factor in the relation (2.5) of $f^* = 1.09$.

In studying the effect of sliding enhanced creep in the outer ring of material PBCQ as mentioned before, it is not entirely clear what value of f^* is appropriate to account for free sliding between the grains surrounding a central grain. This would necessitate a three-dimensional analysis of the grain aggregate. Here we will use the value $f^* = 1.09$ found above for the axisymmetric geometry, and it is noted that this leads to creep rates for the whole aggregate which correspond to using a value $f_0^* = 1.16$ in an overall constitutive relationship based on (2.5).

As discussed in Section 4, the curve in Fig. 6 also serves as a master curve for the value of the enhancement factor g_B in (4.3). For a given applied stress state and a given value of the viscosity, one evalutes $\dot{\varepsilon}_e^C/\dot{\varepsilon}_B$ and reads the corresponding value of g_B from Fig. 6: $g_B = (\dot{E}_1/\dot{\varepsilon}_e^C)^{1/n}$.

5.2. Cavitation on freely sliding inclined boundaries

On the central transverse facet and, when pertinent, also on the inclined grain boundary, all cavities are assumed to be present from the beginning. Moreover, it is assumed that initially they are uniformly distributed over the facet and of equal size. All results to be presented here are based on an initial cavitation state on the transverse facet AP as specified by $(a/b)_I = 0.1$ and $b_I/R_0 = 0.1$. Whenever cavitation at the inclined boundary PQ is considered, the initial cavity size is taken identical to that on the transverse facet, $(a_{PQ}/a_{AP})_I = 1$, with either the same spacing, $(b_{PQ}/b_{AP})_I = 1$, or four times the spacing, $(b_{PQ}/b_{AP})_I = \sin^{-2}\varphi = 4$. The latter spacing is motivated by experimental results concerning the nucleation rate on differently oriented cavitated grain boundaries reported in [3].

The figures show the growth of a/b as a function of the radii T2 ($x^2/R_0 = 0.20$) and T6 ($x^2/R_0 = 0.92$) on the transverse facet AP (see Fig. 3). Cavity growth results for the inclined boundary PQ are presented in the form of the average value at the nodes on either side of the grain boundary which coincided in the undeformed configuration at the positions I2 ($x^1/B_0 = 0.055$), I5 ($x^1/B_0 = 0.43$) and I9 ($x^1/B_0 = 0.945$) as indicated in Fig. 3, respectively.

In Fig. 7 the macroscopic true stresses are specified by $\sigma_1/E = 0.001$ and $\sigma_2/\sigma_1 = 0.5$, so that the macroscopic effective Mises stress is $\sigma_e/E = 0.0005$. Free sliding is assumed along PQ and the grain boundary diffusion parameter $\mathscr{D}$ is specified in terms of L relative to the initial cavity radius on AP by the initial value $(a/L)_I = 0.025$. Here and in the sequel the initial value of L denotes the value obtained by substituting the average effective

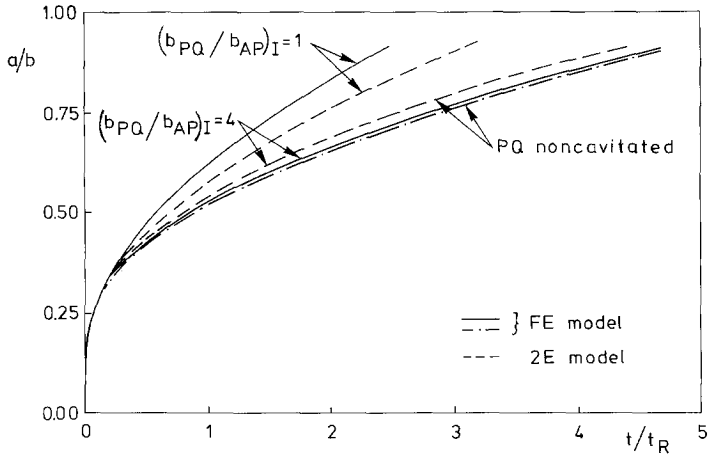

Fig. 7. Cavity growth on the transverse facet at T2 for $(a/L)_I = 0.025$, $\dot{\varepsilon}_e^C/\dot{\varepsilon}_B = 0$ and $\sigma_2/\sigma_1 = 0.5$.

stress into (2.9). The case without cavitation on PQ, as analysed in [9], is shown for comparison.

The full finite element computations in Fig. 7 show that for $(b_{PQ}/b_{AP})_I = 4$ the influence of cavitation at the inclined grain boundary is negligible, while for $(b_{PQ}/b_{AP})_I = 1$ cavity growth on the transverse facet is enhanced considerably. Thus, the time to coalescence of cavities on the transverse facet is reduced by a factor of 2 [16]. In all cases, cavity growth on AP was found to be practically uniform, so that cavity growth results for T6 are virtually indistinguishable from those at T2 as shown in Fig. 7.

Figure 8 shows the cavity growth at the inclined grain boundary for the same case. For both initial uniform cavity spacings, growth is approximately uniform over most of the boundary PQ but decreases towards the triple grain junction Q, as shown by the results for I9, due to the severe constraints on the deformation pattern. Comparing with Fig. 7, it is observed that also in the case of identical initial cavitation states on both facets, $(b_{PQ}/b_{AP})_I = 1$, cavity growth on the inclined facet is slower than that on the transverse facet: $a_{I2}/a_{T2} = 0.74$ at $t/t_R = 2.39$.

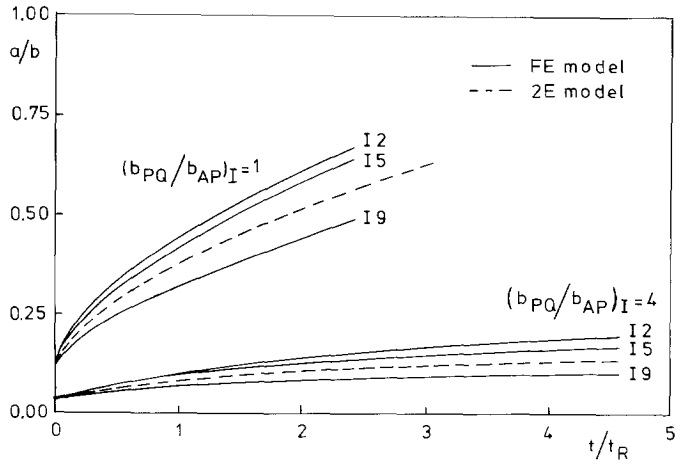

Fig. 8. Cavity growth on the inclined grain boundary for $(a/L)_I = 0.025$, $\dot{\varepsilon}_e^C/\dot{\varepsilon}_B = 0$ and $\sigma_2/\sigma_1 = 0.5$.

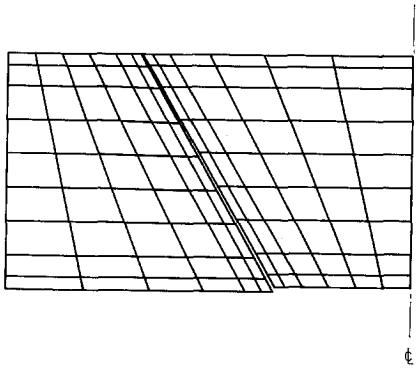

Fig. 9. Deformed mesh corresponding to $(a/L)_I = 0.025$, $\dot{\varepsilon}_e^C/\dot{\varepsilon}_B = 0$, $(b_{PQ}/b_{AP})_I = 1$ and $\sigma_2/\sigma_1 = 0.5$ at $t/t_R = 2.39$.

The predictions of the simple 2E model are shown in Figs. 7 and 8 as well. A value of 1.09 for the enhancement factor g_B in (4.3) is used, which corresponds to free sliding along PQ (see Section 5.1). The uniform cavity growth on both AP and PQ according to that model gives a good approximation of the detailed numerical results. According to the results in Fig. 7 for $(b_{PQ}/b_{AP})_I = 1$, the interaction between the cavitation processes on the two types of facets is underestimated by the simple model.

Figure 9 shows the deformed mesh corresponding to the solution in Figs. 7 and 8 for $(b_{PQ}/b_{AP})_I = 1$ shortly before first coalescence. The combined effect of thickening of the grain boundary layers, owing to cavity growth, and sliding at the inclined grain boundary is clearly seen.

For the cases shown in Figs. 7 to 9, where $(a/L)_I = 0.025$, cavity growth is considerably constrained by the rate of creep of the grains. This is characterized by low values of the normal facet stresses relative to the macroscopic resolved normal stress [9]. Figure 10 shows the cavity growth for a different diffusion parameter specified by $(a/L)_I = 0.33$ but otherwise for identical parameters and an initial cavity spacing on PQ according to $(b_{PQ}/b_{AP})_I = 1$. Here, dislocation creep gives a significant contribution to cavity growth and the creep

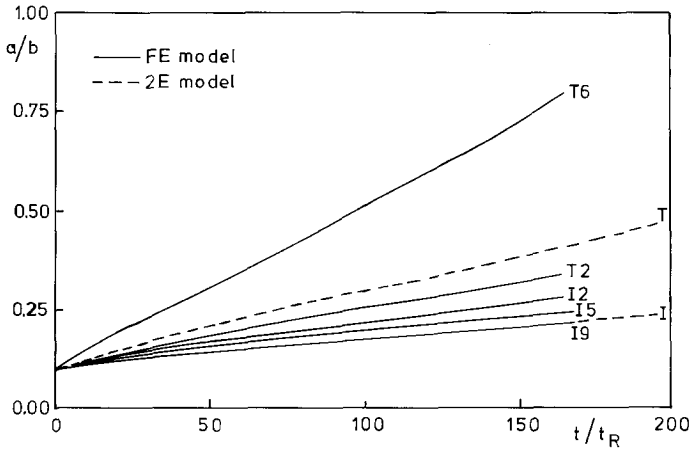

Fig. 10. Cavity growth on transverse and inclined grain boundaries for $(a/L)_I = 0.33$, $\dot{\varepsilon}_e^C/\dot{\varepsilon}_B = 0$ and $\sigma_2/\sigma_1 = 0.5$, and with $(b_{PQ}/b_{AP})_I = 1$.

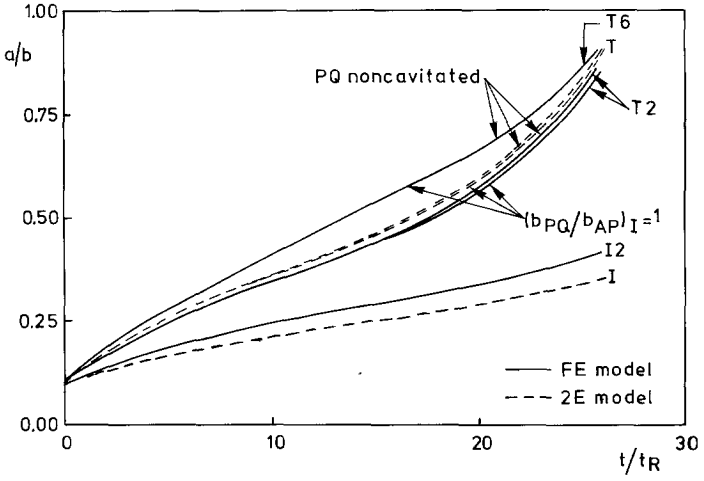

Fig. 11. Cavity growth on transverse and inclined grain boundaries for $(a/L)_I = 0.1$, $\dot{\varepsilon}_e^C/\dot{\varepsilon}_B = 0$ and $\sigma_2/\sigma_1 = 0.5$.

constraint is not active. It is found that cavity growth on the transverse facet is practically unaffected by growth on the inclined boundary. Cavity growth on AP in the absence of cavitation on PQ or in the case $(b_{PQ}/b_{AP})_I = 4$ is indistinguishable from that for $(b_{PQ}/b_{AP})_I = 1$ shown in Fig. 10. In these cases cavity growth on AP is uniform in a large central part while free sliding along PQ promotes a considerably faster growth near the edge P. Cavity growth on PQ is found to be much more uniform. The simple 2E model gives a reasonable prediction of the average cavity growth.

Results for an intermediate value of the diffusion parameter, as specified by $(a/L)_I = 0.1$, are shown in Fig. 11. As opposed to the case considered in Figs. 7 to 9, cavity growth on the inclined grain boundary PQ now slightly reduces the cavity growth rate on the transverse facet, but the time to cavity coalescence on AP is hardly affected. For an initial cavity spacing on PQ specified by $(b_{PQ}/b_{AP})_I = 4$, the influence of cavitation is again negligible.

The interaction between the cavity growth processes on the two types of boundaries found above basically relies on two competitive stress redistribution mechanisms which are necessary to accommodate cavity growth. The first is associated with compatibility of the two grain boundary thickening processes at the triple grain junction P and the second has to ensure compatibility of the axial displacements of CQ and QD. In the cases considered here, where the initial cavitation states on the two types of facets are taken identical, the first accommodation mechanism tends to lead to increased normal stresses on the transverse facet when additional cavitation takes place on the inclined boundary, whereas the second tends to have the opposite effect. Which effect is dominant, depends largely on the rate of diffusion relative to the creep rate specified in terms of $(a/L)_I$ as demonstrated above.

In Figs. 12 and 13 the influence of the macroscopic stress state on the cavity growth processes is studied by considering two different stress ratios σ_2/σ_1. The value of the axial stress σ_1 is adapted accordingly such that the macroscopic effective Mises stress and, as a consequence, the reference time t_R are identical with previous cases considered.

Figure 12 shows results for a uniaxial macroscopic stress specified by $\sigma_2/\sigma_1 = 0$ and $\sigma_1/E = 0.0005$. Comparing with Fig. 7, it is observed that the influence of cavity growth at PQ on growth on the central facet AP is considerably smaller under uniaxial stress; the time

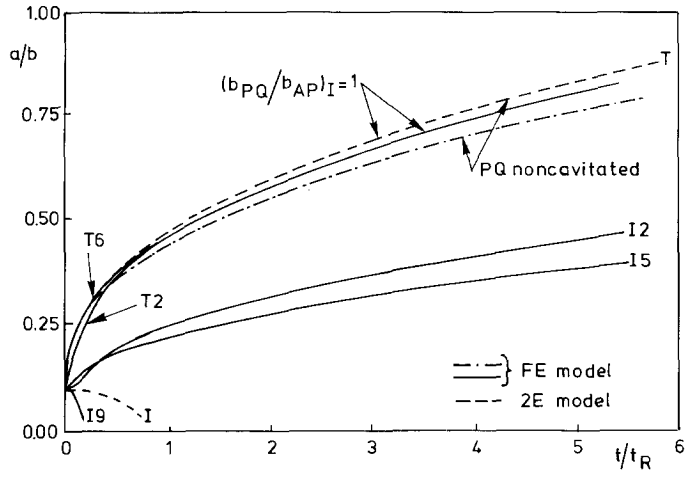

Fig. 12. Cavity growth on transverse and inclined grain boundaries for $(a/L)_I = 0.025$, $\dot{\varepsilon}_e^C/\dot{\varepsilon}_B = 0$ and $\sigma_2/\sigma_1 = 0$.

to coalescence is reduced by only around 20 percent in this case. Cavity growth on the lower half of the inclined boundary, as indicated by I2 and I5, is similar to that in Fig. 8, but at a lower rate. However, in the neighbourhood of the top junction Q, the normal stresses on the inclined boundary are compressive and the cavities that are assumed to be present from the beginning will close down as shown by the curve for I9. Cavity growth on the transverse facet when there is no cavitation along PQ is well predicted by the simple 2E model. As anticipated in Section 4, the influence of cavitation on the inclined boundary cannot be accounted for by the simple model in the present case of a uniaxial stress state. In the simple model, the initial cavities on PQ close down in the early stages of the process due to an average compressive normal stress and, therefore, the small amount of interaction predicted with the elaborate FE model is not represented.

In Fig. 13, where results are shown for a stress state specified by $\sigma_2/\sigma_1 = -0.5$ and $\sigma_1/E = 0.00033$, these trends are even more pronounced. Here compressive normal stresses

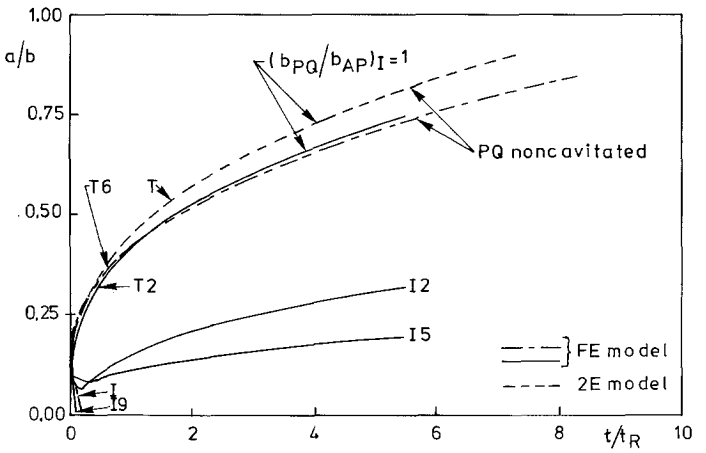

Fig. 13. Cavity growth on transverse and inclined grain boundaries for $(a/L)_I = 0.025$, $\dot{\varepsilon}_e^C/\dot{\varepsilon}_B = 0$ and $\sigma_2/\sigma_1 = -0.5$.

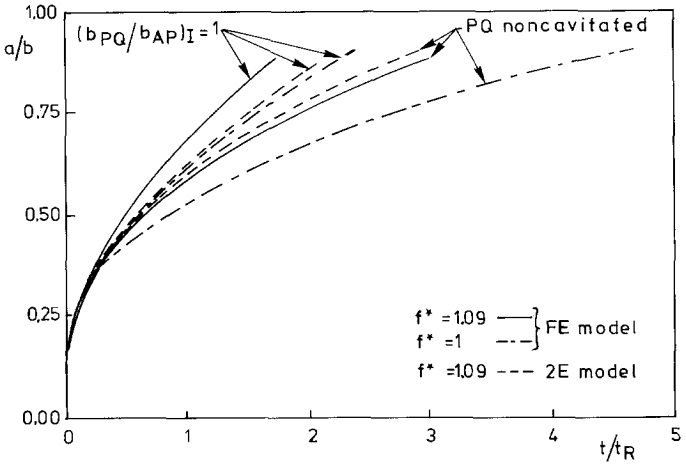

Fig. 14. Cavity growth on the transverse facet at T2 for $(a/L)_I = 0.025$, $\dot{\varepsilon}_e^C/\dot{\varepsilon}_B = 0$ and $\sigma_2/\sigma_1 = 0.5$, with free sliding enhanced creep in the outer ring of material PBCQ.

are predicted on a large part of the inclined boundary. As a consequence, cavity growth on PQ is confined to the neighbourhood of the junction P and its influence on cavity growth on AP is negligible.

In Figs. 14 and 15 we study the effect of free sliding enhanced creep in the outer ring of material, PBCQ, as specified by the value $f^* = 1.09$ discussed in Section 5.1. Figure 14 considers the case of Fig. 7 ($f^* = 1$) in which the creep constraint on cavitation is active. It is observed that due to sliding enhanced creep, the role of cavity growth is significantly increased, so that the time to cavity coalescence on the transverse facet is reduced by about 35 percent. Cavity growth on the inclined boundary is found to be enhanced similarly. The 2E model gives similar approximations of the full computations as in Fig. 7.

In Fig. 15 this effect is considered for the case of Fig. 10 in which cavity growth is not constrained by creep of the surrounding grains. It is observed that also in this case the role of cavity growth is significantly increased by sliding enhanced creep; we estimate the time to

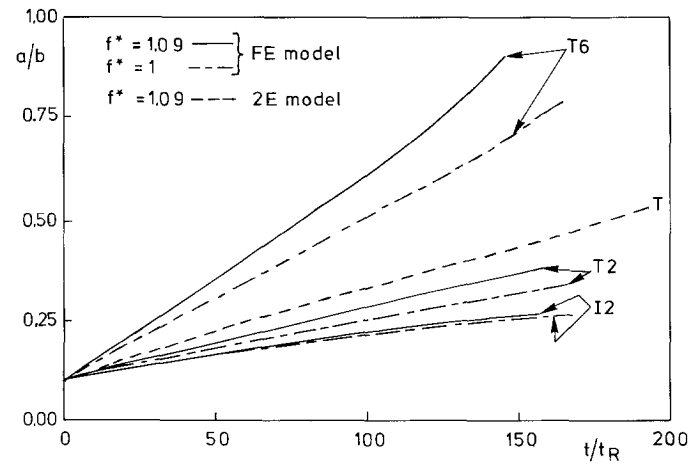

Fig. 15. Cavity growth with free sliding enhanced creep in PBCQ for $(a/L)_I = 0.33$, $\dot{\varepsilon}_e^C/\dot{\varepsilon}_B = 0$ and $\sigma_2/\sigma_1 = 0.5$, and with $(b_{PQ}/b_{AP})_I = 1$.

coalescence on the main facet to be reduced also by around 35 percent. Cavity growth on the inclined boundary is hardly affected by enhanced creep.

5.3. *Effect of grain boundary viscosity*

So far we have considered cases where grain boundary sliding is completely free. Tvergaard [8], using a different numerical model, studied the opposite limiting case where there is absolutely no sliding on grain boundaries adjacent to the central cavitating facet. In the present analysis we can simulate the no sliding condition by taking a sufficiently high value of the viscosity, e.g., the value specified by $\log(\dot{\varepsilon}_e^C/\dot{\varepsilon}_B) = 3.5$ (see Fig. 6). Accordingly, the enhancement factor in the 2E model is $g_B = 1$. Figure 16 shows the cavity growth results for this value of $\dot{\varepsilon}_e^C/\dot{\varepsilon}_B$, with otherwise identical parameters as in Figs. 7 and 8. In the absence of cavitation on PQ, the time to cavity coalescence is around 6 times that in the free sliding case of Fig. 7, as found also in [8, 9]. Cavity growth on the inclined boundary now has a drastic influence on cavity growth on the main transverse facet; with $(b_{PQ}/b_{AP})_I = 1$ the time to coalescence is reduced by a factor of about 5. Comparing with Fig. 8 it is seen that cavity growth on PQ relative to that on AP is considerably faster when there is no sliding on PQ. Cavity growth on PQ clearly relaxes the geometric constraints at the grain junction P which otherwise are observed to give rise to quite a nonuniform cavity growth on the transverse facet in the absence of sliding. This effect also underlines the fact that, as shown in Fig. 16, the simple 2E model gives very good agreement with the full FE calculations when PQ is cavitating, whereas it predicts no growth at all in the absence of cavity growth on PQ.

Figure 17 shows similar results for the case corresponding to Fig. 10 where the creep constraint on cavitation is not active. Just as in the case of free sliding, Fig. 10, cavity growth on PQ is found to have virtually no effect on growth rate on the central facet. Although the cavity growth rate on AP is drastically reduced by suppressing grain boundary sliding, the growth rate on PQ is hardly affected. The predictions of the simple model in the presence of cavity growth on PQ are in excellent agreement, except at the final stage of growth where finite strain effects (not accounted for in the simple 2E model) become important.

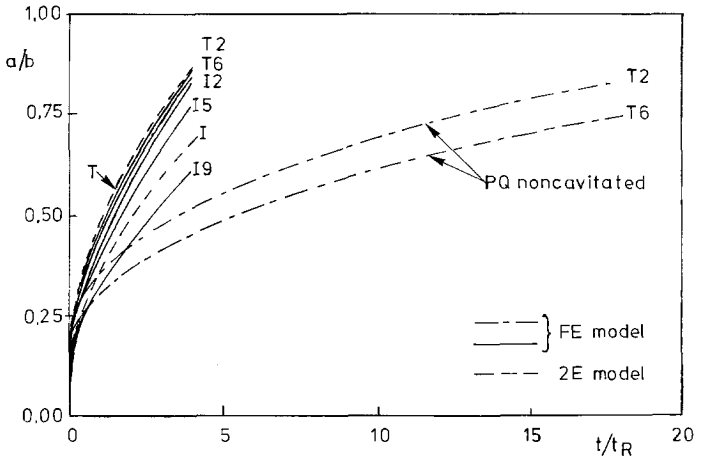

Fig. 16. Cavity growth on transverse and inclined grain boundaries for $(a/L)_I = 0.025$, $\log(\dot{\varepsilon}_e^C/\dot{\varepsilon}_B) = 3.5$ and $\sigma_2/\sigma_1 = 0.5$, with $(b_{PQ}/b_{AP})_I = 1$.

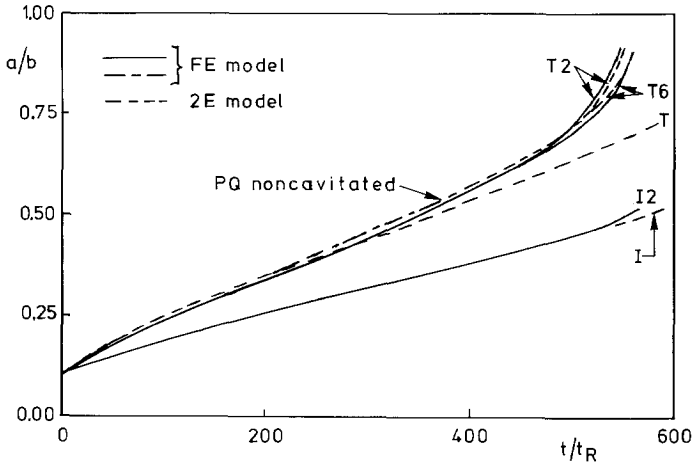

Fig. 17. Cavity growth on transverse and inclined grain boundaries for $(a/L)_I = 0.33$, $\log(\dot{\varepsilon}_e^C/\dot{\varepsilon}_B) = 3.5$ and $\sigma_2/\sigma_1 = 0.5$, with $(b_{PQ}/b_{AP})_I = 1$.

In Fig. 18 cavity growth results are shown for a grain boundary viscosity specified by $\log(\dot{\varepsilon}_e^C/\dot{\varepsilon}_B) = 0.25$, which represents an intermediate case between free sliding and no sliding. According to Fig. 6, this viscosity corresponds to $\dot{E}_1/\dot{\varepsilon}_e^C = 1.27$, so that the value of g_B to be used in (4.3) is $g_B = 1.049$. The results of Fig. 18 are in many respects in between those for free sliding in Figs. 7 and 8 and those for no sliding in Fig. 16. In particular, cavity growth on PQ with $(b_{PQ}/b_{AP})_I = 1$ enhances the cavity growth rate on the transverse facet by a factor of about 4, while for free and no sliding this factor was found to be 2 and 5 respectively. The results are well approximated by the simple model, also in the absence of cavitation on PQ.

In Fig. 19 some of the previous results for $(a/L)_I = 0.025$ and $\sigma_2/\sigma_1 = 0.5$ are replotted to summarize the influence of the various mechanisms considered in this paper, regarding cavity growth rates on transverse grain boundary facets. According to this figure the time to failure in the presence of cavitation at freely sliding inclined grain boundaries, taking into account free sliding enhanced creep (curve E), is around 20 times less than the failure time in the absence of sliding and with no cavitation at inclined boundaries (curve A).

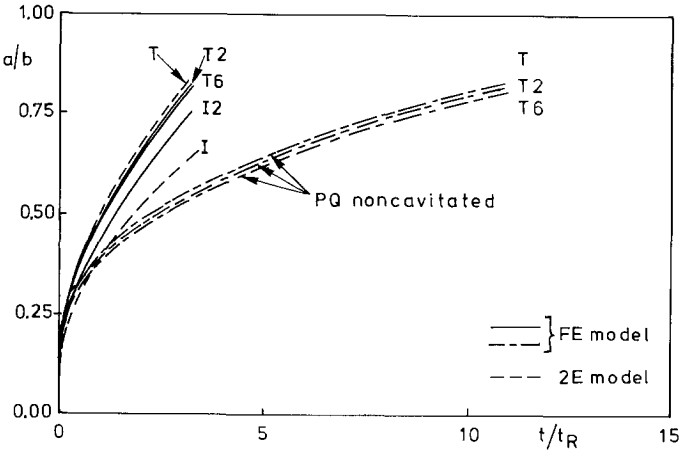

Fig. 18. Cavity growth on transverse and inclined grain boundaries for $(a/L)_I = 0.025$, $\log(\dot{\varepsilon}_e^C/\dot{\varepsilon}_B) = -0.25$ and $\sigma_2/\sigma_1 = 0.5$, with $(b_{PQ}/b_{AP})_I = 1$.

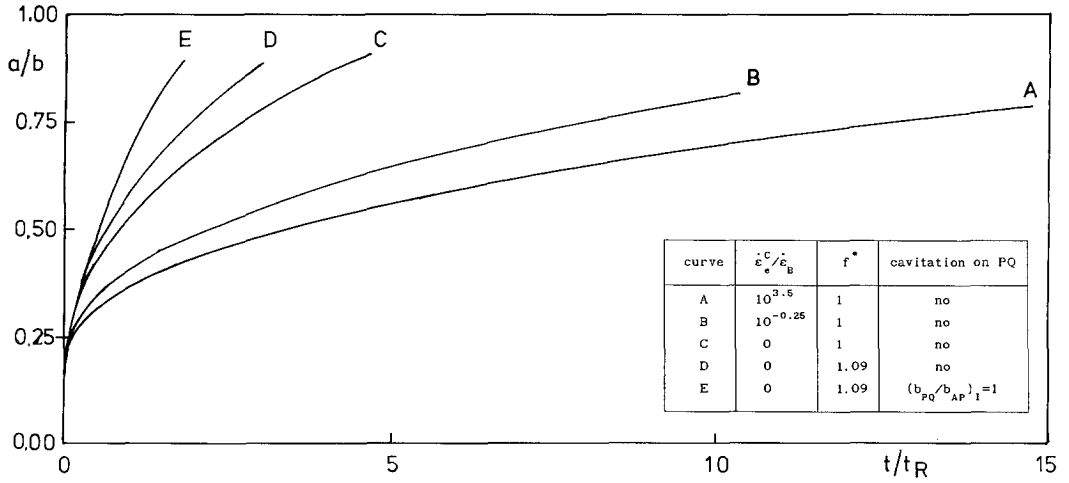

Fig. 19. Cavity growth at T2 on the transverse grain boundary facet for $(a/L)_I = 0.025$ and $\sigma_2/\sigma_1 = 0.5$, with various sliding and cavitation conditions on the inclined grain boundary.

All finite element results presented in this paper are obtained using the mesh shown in Fig. 3. This mesh may not be fine enough to accurately capture the details of the process in the immediate vicinity of the triple grain junctions, but on the basis of experience in previous studies, the mesh in Fig. 3 is considered sufficient for the present purpose. In the study [8] of cavitation without grain boundary sliding it was found that the rupture times increased only a few percent by using around half the number of elements. Also in studying the effect of grain boundary sliding alone [14], it was found that a much cruder mesh increased the total rupture times only slightly.

6. Discussion

Analyses of creep failure by grain boundary cavitation have mainly focused on cavity growth and coalescence at grain boundary facets normal to the maximum principal tensile stress, thus implying that failure processes on adjacent inclined facets are of secondary importance. However, the model studies in the present paper show that progressive failure on such adjacent inclined facets may strongly reduce the time to first coalescence on transverse facets. This effect is not seen in the range of material parameters where diffusion is less dominant so that there is no creep constraint on the rate of cavitation. However, when diffusion is sufficiently rapid to give creep constrained cavitation, the occurrence of cavity growth on inclined sliding grain boundaries relaxes the normal stresses on these boundaries, thus accelerating cavity growth on the transverse facets.

In all cases analysed here, the first formation of a grain boundary micro-crack by cavity coalescence occurs at a transverse facet whose normal is in the direction of the maximum principal tensile stress. Based on these results it appears that the time to cavity coalescence on transverse facets is a relevant lower bound measure of the material lifetime, in spite of the simultaneous occurrence of failure processes on the adjacent inclined facets. As noted by Riedel [12] the onset of failure processes in the material around a grain boundary facet subject to creep constrained cavitation will not await the formation of an open micro-crack,

because the stress states before and after coalescence are virtually identical. Riedel [12] expects that this makes the time to coalescence irrelevant as a measure of the life-time; but the present results show the opposite. The main point is that the usual simple models of cavitation on a single grain boundary facet may give a strongly non-conservative life-time estimate, because the time to coalescence may be significantly overestimated if the interaction with failure processes on the adjacent inclined facets is neglected.

In studies of the effect of free grain boundary sliding there is a significant difference between plane strain models and 3D models. For a planar hexagonal array of grains (see [19, 20]) with micro-cracks formed at all grain facets normal to the maximum tensile stress, free sliding at all other grain boundaries will lead to immediate failure without any deformation of the grains, while in a 3D array of grains creep deformations are needed to accommodate sliding off [13, 14]. The axisymmetric model problem used in the present investigation (see also [9, 16]) does require an accommodating deformation mechanism for the grains in the form of truncated cones. However, the effect of sliding is not automatically included in the outer ring of material representing a number of grains surrounding the two central grains of the model. The computations using a stress enhancement factor in the outer ring of material to represent free sliding of the surrounding grains relative to one another show that this increases the rate of cavity growth on the transverse facet, both in the creep constrained range and the unconstrained range. The stress enhancement factor used for the outer ring in the present computations results in overall creep rates corresponding to an overall stress enhancement factor of about 1.16. It is noted that this value is of the order of the value 1.2 found by Ghahremani [20] for a planar array of grains, but somewhat lower than the value 1.26 recently found by Rodin and Dib [28] based on a full three-dimensional finite element analysis for an array of grains in the form of Wigner-Seitz cells.

Most of the analyses in the present paper focus on the effect of free grain boundary sliding, as has also been the case in previous investigations [9, 13, 16], but also a few cases with non-zero grain boundary viscosity are considered. For a very high grain boundary viscosity, sliding is essentially prevented; but it is interesting to note that cavitation on the inclined grain boundaries may still have a significant effect on the time to coalescence. Thus, in the range of creep constrained cavitation the rate of cavity growth on transverse facets is much increased by the occurrence of cavities on the non-sliding adjacent inclined facets, whereas the occurrence of such cavities on inclined facets has negligible influence in the unconstrained cavitation range. For an intermediate value of the grain boundary viscosity, which allows for some sliding but does not completely relax the shear stresses on the boundary, the reductions of the time to coalescence due to sliding and cavitation on inclined boundaries are in between the reductions found for free sliding and for no sliding, respectively.

The cavity growth model used in the present paper accounts for the effect of diffusion as well as dislocation creep of the surrounding material. This model has been developed for grain boundaries normal to the maximum tensile stress. At sliding grain boundaries the development of non-equilibrium void shapes may accelerate growth, but according to Chen [24] models neglecting this effect by assuming quasi-equilibrium void shapes are reasonable approximations for relatively low sliding rates. Another approximation in the present analysis is that the commonly observed continuous nucleation of cavities during the creep process is neglected by assuming that all cavities are present from the start. Nucleation has been neglected here to focus on other effects, but based on previous investigations that incorporate continuous nucleation [9] it is expected that the conclusions of the present investigation will essentially hold in the presence of nucleation.

The 2E model developed in Section 4 is in a number of ways oversimplified relative to the full FE cell model analysis. The main limitation of the 2E model is that it accounts only for uniform stress and cavitation states at the grain boundaries. However, comparison of the predictions obtained by the simple 2E model with those based on the more elaborate FE analysis shows that in most cases the main features of the material behaviour are captured by this simple model.

Acknowledgements

The research of EvdG was made possible by a fellowship of the Royal Netherlands Academy of Arts and Sciences. The major part of this research was carried out when he was associated as a visiting research fellow with the Department of Solid Mechanics of the Technical University of Denmark.

Appendix A

Subdivision into grain boundary elements

Due to grain boundary sliding, the grain boundary layer must be re-subdivided into grain boundary elements at each increment during the incremental procedure. In brief, the algorithm is as follows (see Fig. 4):

1. For each node of the quadrilateral elements adjacent to the grain boundary layer, "phantom nodes" are introduced on the opposite face. The phantom node b' corresponding to b, for instance, is defined as the average of the points obtained by projecting b onto cd either orthogonal to ab or orthogonal to the face of the other element b belongs to. If these two projections fall on the faces of two adjacent elements, the phantom node is taken to coincide with the common nodal point of these elements.
2. The midpoint of a line connecting a node and its phantom node, e.g., point q on the line bb', serves as a grain boundary node. Lines connecting adjacent grain boundary nodes, e.g. pq, define the discrete midplane of the grain boundary.
3. The typical element shown in Fig. 4 is then defined as the segment of the grain boundary layer between the grain boundary nodes p and q bounded by the faces bb' and cc'. In the calculations presented here, the boundary faces bb' and cc' remain approximately perpendicular to the midplane.

Appendix B

Governing equations of the 2E model

Equilibrium of the simplified model shown in Fig. 5 is expressed by the virtual work condition (summation over α)

$$\pi A_0^2 \sigma_1 \delta U_{\mathrm{I}} + 2\pi A_0 B_0 \sigma_2 \delta U_{\mathrm{II}} = \pi R_1^2 B_0 \sigma_{\alpha c} \delta \varepsilon_{\alpha c} + \pi (A_0^2 - R_1^2) B_0 \sigma_{\alpha r} \delta \varepsilon_{\alpha r}$$
$$+ \pi R_0^2 \sigma_{nt} \delta \delta_t + 2\pi R_1 B_0 / \cos\varphi (\sigma_{ni} \delta \delta_i + \tau \delta \gamma), \tag{A.1}$$

where σ_1 and σ_2 are the applied macroscopic stresses. Substitution of the expressions similar to (4.1–2) for the virtual strains in terms of the virtual displacements δU_{I}, δU_{II}, δu_c^2, δu_r^2 and $\delta\delta_t$ then yields the following 5 equilibrium equations:

$$
\begin{aligned}
\sigma_1 &= \left(\frac{R_1}{A_0}\right)^2 \sigma_{1c} + \left[1 - \left(\frac{R_1}{A_0}\right)^2\right] \sigma_{1r}, \\
\sigma_2 &= \frac{1}{2}\left(1 + \frac{R_1}{A_0}\right) \sigma_{2r} + \frac{1}{2}\left(1 - \frac{R_1}{A_0}\right) \sigma_{3r}, \\
0 &= -\frac{1}{2}\left(1 + \frac{R_1}{A_0}\right) \sigma_{2r} + \frac{1}{2}\left(1 - \frac{R_1}{A_0}\right) \sigma_{3r} + \frac{R_1}{A_0}(\sigma_{ni} + \tau \tan\varphi), \\
0 &= \sigma_{2c} - (\sigma_{ni} + \tau \tan\varphi), \\
0 &= -\left(\frac{R_1}{A_0}\right)^2 \sigma_{1c} + \left(\frac{R_0}{A_0}\right)^2 \sigma_{nt} + \frac{R_1}{A_0}\frac{B_0}{A_0}(\sigma_{ni} \tan\varphi - \tau).
\end{aligned}
\tag{A.2}
$$

The rate equilibrium conditions are obtained by straightforward differentiation (recall that nonlinear geometric effects are neglected). Eliminating the stress-rates and strain-rates by the constitutive equations for the creeping grains and the grain boundaries and the definitions (4.1–2), a typical displacement finite element system of equations results for the unknowns $\dot{U}_{\mathrm{I}}$, $\dot{U}_{\mathrm{II}}$, $\dot{u}_c^2$, $\dot{u}_r^2$ and $\dot{\delta}_t$. Using (A.2) as an equilibrium correction, the system of equations is similar in form to that of the FE model, and hence, can be solved in much the same way.

References

1. D. Hull and D.E. Rimmer, *Philosophical Magazine* 4 (1959) 673–687.
2. A.C.F. Cocks and M.F. Ashby, *Progress in Materials Science* 27 (1982) 189–244.
3. A.S. Argon, in *Recent Advances in Creep and Fracture of Engineering Materials and Structures*, B. Wilshire and D.R.J. Owen (eds.), Pineridge Press, U.K. (1982) 1–52.
4. A. Needleman and J.R. Rice, *Acta Metallurgica* 28 (1980) 1315–1332.
5. T.-L. Sham and A. Needleman, *Acta Metallurgica* 31 (1983) 919–926.
6. B.F. Dyson, *Metal Science* 10 (1976) 349–353.
7. J.R. Rice, *Acta Metallurgica* 29 (1981) 675–681.
8. V. Tvergaard, *Journal of the Mechanics and Physics of Solids* 32 (1984) 373–393.
9. V. Tvergaard, *Journal of the Mechanics and Physics of Solids* 33 (1985) 447–469.
10. A.C.F. Cocks and F.A. Leckie, *Advances in Applied Mechanics* 25 (1987) 239–294.
11. H. Riedel, *Fracture at High Temperatures*, Springer, Berlin (1986).
12. H. Riedel, *Zeitschrift für Metallkunde* 76 (1985) 669–675.
13. P.M. Anderson and J.R. Rice, *Acta Metallurgica* 33 (1985) 409–422.
14. V. Tvergaard, *International Journal of Solids and Structures* 21 (1985) 279–293.
15. V. Tvergaard, *Revue de Physique Appliquée* 23 (1988) 595–604.
16. E. van der Giessen and V. Tvergaard, in *Mechanics of Creep Brittle Materials 1*, A.C.F. Cocks and A.R.S. Ponter (eds.), Elsevier Applied Science (1989) 277–289.
17. M.F. Ashby, *Surface Science* 31 (1972) 498–542.
18. R. Raj and M.F. Ashby, *Metallurgical Transactions* 2 (1971) 1113–1127.
19. F.W. Crossman and M.F. Ashby, *Acta Metallurgica* 23 (1975) 425–440.
20. F. Ghahremani, *International Journal of Solids and Structures* 16 (1980) 847–862.

21. B.F. Dyson, *Scripta Metallurgica* 17 (1983) 31–37.
22. I.-W. Chen and A.S. Argon, *Acta Metallurgica* 29 (1981) 1321–1333.
23. I.-W. Chen, *Scripta Metallurgica* 17 (1983) 17–22.
24. I.-W. Chen, *Metallurgical Transactions* 14A (1983) 2289–2293.
25. D. Pierce, C.F. Shih and A. Needleman, *Computers and Structures* 18 (1984) 875–887.
26. V. Tvergaard, *Acta Metallurgica* 32 (1984) 1977–1990.
27. B.F. Dyson, *Revue de Physique Appliquée* 23 (1988) 605–613.
28. G.J. Rodin and M.W. Dib, in *Advances of Fracture Research*, ICF7, K. Salama et al. (eds.), Vol. 2, Pergamon Press (1989) 1835–1842.